Thermal Characteristics Investigation of Lithium-Ion Battery Under High-Frequency AC Excitation in Low-Temperature Environment

Zhongxiaobang Hu, Yang Li, *Member, IEEE*, Furong Liu, *Member, IEEE*, Bo Zhao, *Member, IEEE*, Weibo Li, *Member, IEEE*, Ruixin Yang, *Member, IEEE*, Changjun Xie, *Member, IEEE*, and Ying Shi

***Abstract*— At low operating temperatures, the power capability and charging/discharging capacity of lithium-ion (Li-ion) batteries can decay rapidly. Therefore, it is essential to preheat the Li-ion batteries in advance of the normal operations of a battery electric vehicle. High-frequency ac preheating methods are advantageous to achieve a miniaturized and lightweight design. In this article, a self-heating circuit topology is used for studying the characteristics of Li-ion batteries at low temperatures and under high-frequency ac excitation. The thermal behaviors of Li-ion batteries under high-frequency ac excitations are comprehensively analyzed with an improved heat generation model. Experimental results exhibit that heat generation due to electrochemical reactions has a significant influence on self-heating rates under the high-frequency ac excitation, and the heating rate is positively correlated with the current frequency and root-mean-square (rms) value. Specifically, when the current frequency is 90 kHz and the rms value is 3.51 A or 1.17 C, validated by experiment and numerical simulation, a 2.9-Ah 18650 Li-ion cell can be heated up from −20 °C to 5 °C in 7.33 min with an average electrochemical heat generation of 2.962 W.**

***Index Terms*— Electric vehicles (EVs), high-frequency ac heating, lithium-ion (Li-ion) batteries, low temperature, thermal characteristics.**

I. Introduction

THE flourishing of electric vehicles (EVs) is an important measure taken by countries around the world to promote the development of green and sustainable energy [1], [2]. Due to its high energy density, no memory effects, and environment-friendly nature, lithium-ion (Li-ion) battery has become the primary power source and energy storage technology for EVs [3]–[5]. However, large deployment of EVs has been hindered by the derated performance of the Li-ion batteries in the low-temperature environment: the energy storage capacity, charging/discharging capability, and lifespan of Li-ion batteries are all reduced, which causes the problems of decreased driving mileage, lowered power rating, and growing range anxiety [6], [7]. For example, when the temperature drops below −20 °C, the drastic increase in battery internal resistance can lead to significant losses of pulse power capability and available energy [8]–[11]. Furthermore, at extremely low temperatures, cold starting or fast charging a Li-ion battery can trigger degradation phenomena, such as lithium deposition, and cause safety hazards due to internal short circuits [12]. To solve these critical problems, research efforts have been made to improve the thermal characteristics of different battery components, including the electrolyte cosolvent, electrolyte salt, and the active materials of the cathode and anode [13]. Unfortunately, the improvements on battery performance at low temperatures are still limited based on prevailing battery design, and more cost-effective solutions are needed for practical applications.

A more direct and well-accepted pathway is to design a heating device and corresponding control strategies for EV applications, such as cold start and fast charging. Under low-temperature conditions, if the battery can be quickly preheated to the normal operating temperature prescribed by the battery manufacturer, its excellent performance can be regained, and accelerated aging can be prevented [14]. Hence, in recent years, many research efforts have been devoted to developing various strategies for preheating Li-ion batteries in a cold climate, which can be generally categorized as *external heating* and *internal heating*.

External heating uses an external heat source to warm up the batteries by means of convection or conduction, and it is currently adopted by most commercial EVs. For example, the batteries can be preheated by conduction using an electric heating film [15] or by convection using air or liquid as the heat transfer medium [16], [17]. However, due to the long heat transfer path, external heating has the disadvantages of low heating efficiency, high energy consumption, and long heating time, and it can lead to significant temperature nonuniformity across the battery pack [18]. In addition, the performance of the external heating usually depends heavily on the external

Manuscript received June 7, 2021; revised July 26, 2021 and September 3, 2021; accepted September 13, 2021. Date of publication September 20, 2021; date of current version March 22, 2022. This work was supported in part by the National Key Research and Development Program of China under Grant 2020YFB1506802, in part by the National Natural Science Foundation of China under Grant 51977164, and in part by the Hubei Provincial Key Research and Development Program under Grant 2020BAB131. *(Corresponding authors: Furong Liu; Ruixin Yang; Changjun Xie.)*

Zhongxiaobang Hu is with the School of Automation, Wuhan University of Technology, Wuhan 430070, China (e-mail: huzhongxb@whut.edu.cn).

Yang Li, Furong Liu, Weibo Li, Changjun Xie, and Ying Shi are with the School of Automation, Wuhan University of Technology, Wuhan 430070, China (e-mail: yang.li@whut.edu.cn; lfr@whut.edu.cn; liweibo@whut.edu.cn; jackxie@whut.edu.cn; a_laly@163.com).

Bo Zhao is with the State Grid Zhejiang Electric Power Research Institute, Hangzhou, Zhejiang 310014, China (e-mail: zhaobozju@163.com).

Ruixin Yang is with the Department of Vehicle Engineering, School of Mechanical Engineering, Beijing Institute of Technology, Beijing 100081, China (e-mail: yangruixin@bit.edu.cn).

Digital Object Identifier 10.1109/TTE.2021.3113945

thermal management strategies. Various factors, such as the type and the geometric design of the battery pack, have also to be taken into consideration to properly balance the heating efficiency, energy consumption, and temperature uniformity, which makes the external heating complex to design and inflexible to implement.

In contrast, internal heating uses Joule heat and reaction heat generated by the current flowing through the battery as the heating source [19], [20]. Hence, the temperature distribution is more uniform than the external heating methods. Also, since the long heat conduction path in the internal heating is avoided in the design, the thermal loss can be reduced, and energy utilization can be increased [8], [17]. To achieve internal heating, some studies focus on the modification of the internal battery design by adding extra components. For example, Yang *et al.* [21] proposed an all-climate battery, where a metal foil is inserted into the cell to generate a large amount of heat under pulse discharge and charging conditions. Zhang *et al.* [22] proposed to insert two foils to significantly increase the heating rate, while the foil can also be used as an internal temperature sensor. However, adding foils to the battery cells requires a change of battery structure, which incurs additional costs in manufacturing, packaging, and management. Hence, it is more economically viable to design and implement an external heating circuit to achieve internal heating,

Heating methods can also be divided into dc heating and ac heating. For dc heating, the current amplitude and duration must be controlled properly within a certain range to avoid low heating rates and weak preheating effects caused by lithium deposition [8], [17]. Qin *et al.* [23] used bidirectional pulse currents to heat the Li-ion batteries rapidly, and reduced lithium deposition was observed by applying negative pulse currents with a larger amplitude than the positive pulse current. Mohan *et al.* [24] developed a predictive-control-based technique to minimize energy loss with optimized bidirectional currents. In the meantime, a large number of studies have shown that ac heating has little damage to the battery pack, and it is regarded as the most promising technology for EV preheating [25]. Ruan *et al.* [26] proposed a low-temperature fast heating strategy, where a high heating rate was achieved by maintaining a sinusoidal ac polarization voltage. Ge *et al.* [27] based on the maximum ac magnitude without lithium deposition at each temperature, developed a temperature-adaptive, deposition-free ac preheating method.

However, most of these ac preheating methods use the external power to generate the current to heat the battery, which significantly limits the applications for practical use. In order to generate the heating current in ac form by efficiently utilizing the energy stored in the battery, Jiang *et al.* [28] designed a soft-switching resonant circuit based on H-bridge to generate ac and dc superimposed currents to heat the battery pack. The energy loss of the battery is only 6.64%. Shang *et al.* [29], thus, designed a high-frequency sine-wave heater based on resonant *LC* converters to self-heat the automotive batteries from −20°C to 0 °C within 3.1 min. Although the above two self-heating circuits based on the H-bridge can use the energy of the battery to generate alternating current for preheating, the frequency and the rms value of the alternating current are determined by the parameters of the *LC* converters, which reduces the flexibility of the design amenable for various practical operating conditions since those two parameters are relatively fixed. In this study, we improve the heating method based on the H-bridge circuit, while the frequency of the ac heating current and the rms current value can be readily adjusted. A preheating circuit based on the H-bridge is first proposed to study the thermal characteristics of Li-ion batteries under high-frequency excitation. The circuit uses the battery as the power source to generate ac excitation for self-heating, and the requirement on an external source is avoided. This is the first contribution of this work.

Model-based methods are effective to investigate the behaviors of the preheating system, and a thermal model that describes the heat generation and heat transfer in the battery pack has been widely used in the above works. However, the Bernard heat generation model only shows that the heat generation is positively correlated with the root-mean-square (rms) current value and the internal resistance of the battery, where the influence of the preheating current frequency is missing [30]. Ruan *et al.* [26] and Ge *et al.* [27] pointed out that, with the increase in the heating current frequency, the Joule heat generated by the internal resistance of the battery decreases, so it is recommended to choose a lower ac frequency to increase the heating speed. On the contrary, Ji and Wang [17] show that high-frequency ac signals could accelerate the heating process, and a similar conclusion is drawn in [31]. These two diametrically opposed conclusions motivate our present investigation on the thermal characteristics of Li-ion batteries under high-frequency ac excitation. In the present investigation, experimental studies have been conducted to verify a derived relationship between the electrochemical heat generation, the frequency, and the rms current value when high-frequency ac is used to heat the battery. By comparing the effects of different frequencies and different rms current values on the heating rates, guidelines for designing a scheme for preheating the battery under high-frequency ac excitation are established for a practical system. This forms the second major contribution of this work.

The remainder of this article is organized as follows. In Section II, the topology and operating principles of the heating circuit are introduced, the analytical expression of the heating current rms is derived, and a new high-frequency heat generation model of the battery is established. Section III describes the experimental device briefly and introduces the acquisition methods of relevant experimental parameters. In Section IV, the experimental results and discussion about internal heating are presented in detail, and the model is verified and analyzed. Section V summarizes the main findings of the work.

II. Design of Self-Heating Scheme for Power Battery

A. Experimental Circuit and Operating Principles

Fig. 1 shows the topology of the self-heating circuit for the battery pack under investigation. The circuit consists of

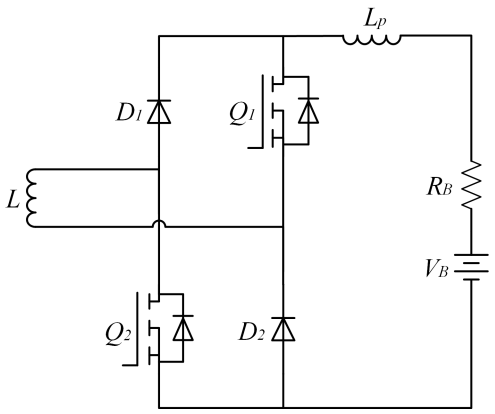

Fig. 1. Topology of the H-bridge high-frequency ac heating circuit.

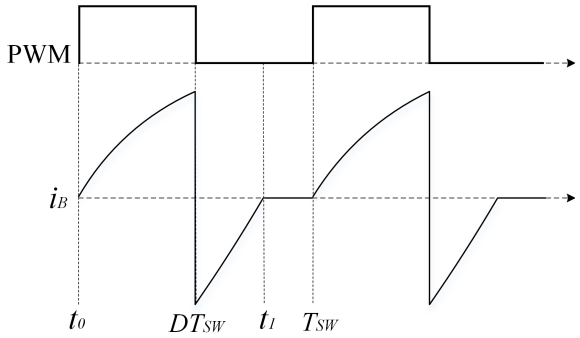

Fig. 2. Waveforms of the H-bridge heating circuit.

two switches (Q_1 and Q_2), two diodes (D_1 and D_2), a series inductor L, and a parasitic inductance L_P. The switches are driven by a pulsewidth modulation (PWM) signal with adjustable frequencies and duty cycles. The battery pack is represented by a dc source V_B and an internal resistance R_B.

Fig. 2 presents the theoretical working waveforms of the heating circuit. The heating circuit has two operating modes in one switching period $T_{\rm SW}$, and corresponding equivalent circuits are shown in Fig. 3.

Mode 1: As shown in Fig. 3(a), at $t = t_0$, the switches Q_1 and Q_2 are turned on, the diodes D_1 and D_2 are turned off, and the battery is in the discharge mode. Due to the presence of the series inductance L and the parasitic inductance L_P, the discharge current increases slowly. In this operating mode, heat is generated due to the internal resistance and chemical reaction of the battery. The discharge current can be adjusted by controlling the switching frequency $f = 1/T_{\rm SW}$ and duty cycle D of the switches.

Mode 2: As shown in Fig. 3(b), at $t = {\rm DT_{SW}}$, Q_1 and Q_2 are turned off, D_1 and D_2 are turned on, and the battery pack is being charged and heated by the energy released from the inductors.

It can be seen that the heating circuit can make full use of the self-discharge energy of the battery and the discharge energy of the inductor to heat the battery pack. It should be pointed out that the amplitudes of the currents flowing through the battery pack in Mode 1 and Mode 2 are the same, and the directions are opposite, so the strategy can be regarded as an ac preheating method for the battery pack.

B. Derivation of RMS Value of Heating Current

Mode 1: According to KVL, we have

$$V_B - i_B R_B = (L_P + L)\frac{di_B}{dt} \tag{1}$$

where i_B is the current flowing through the battery pack and other symbols are explained in Section II-A.

At $t = 0$, the current is $i_B = 0$. At $t = {\rm DT_{SW}}$, the current $i_B = V_B/R_B$. Hence, during the interval $0 \le t < {\rm DT_{SW}}$, the current $i_B(t)$ can be expressed as

$$i_B(t) = \frac{V_B}{R_B}\left(1 - \exp\left(-\frac{R_B}{L_P + L}t\right)\right). \tag{2}$$

Under the high-frequency conditions, t is much smaller than the time constant $(L_P + L)/R_B$ of the circuit. This leads to $1 - \exp(-x) \approx x$, and thus, (2) can be approximated by

$$i_B(t) = \frac{V_B}{L_P + L}t. \tag{3}$$

Mode 2: In this mode, the direction of the current i_B is opposite to that in Mode 1. According to KVL, we have

$$V_B + i_B R_B = -(L_P + L)\frac{di_B}{dt}. \tag{4}$$

It should be pointed out that, at the time instant after the switch is turned off, i.e., $t = {\rm DT_{SW}^+}$, the directions of the currents in L and L_P are opposite, and the rates of change of these two currents (i.e., di_B/dt and di_{Lp}/dt) are different. The presence of L_P will hinder the reversion of the heating current direction and reduce the peak value of the reversed current. The experimental results verified that this process is very fast, and there is only a small reduction in the peak current. Therefore, the influence of the parasitic inductance on the calculated rms value of the current can be ignored. Here, we consider that, at $t = {\rm DT_{SW}}$, $i_B \approx -\frac{V_B}{R_B}\left(1 - \exp\left(-\frac{R_B}{L_P + L}{\rm DT_{SW}}\right)\right)$, and at $t = T_{\rm SW}$, $i_B = 0$. Hence, during the time interval ${\rm DT_{SW}} \le t < T_{\rm SW}$, $i_B(t)$ can be expressed as

$$i_B(t) = -\frac{V_B}{R_B}\left(2 - \exp\left(-\frac{R_B}{L_P + L}{\rm DT_{SW}}\right)\right) \times \exp\left(-\frac{R_B}{L_P + L}(t - {\rm DT_{SW}})\right) + \frac{V_B}{R_B}. \tag{5}$$

Similarly, under the high-frequency condition, by applying the Taylor expansion to (5) at $t = 0$, we have $e^x \approx 1 + x$. Therefore, (5) is reduced to

$$i_B(t) = -\frac{V_B}{L_P + L} \cdot \left(1 + \frac{R_B}{L_P + L} \cdot {\rm DT_{SW}}\right)(t - {\rm DT_{SW}}) + \frac{V_B}{L_P + L} \cdot {\rm DT_{SW}}. \tag{6}$$

Combining (2) and (5) yields the expression of the current i_B flowing through the battery pack within a

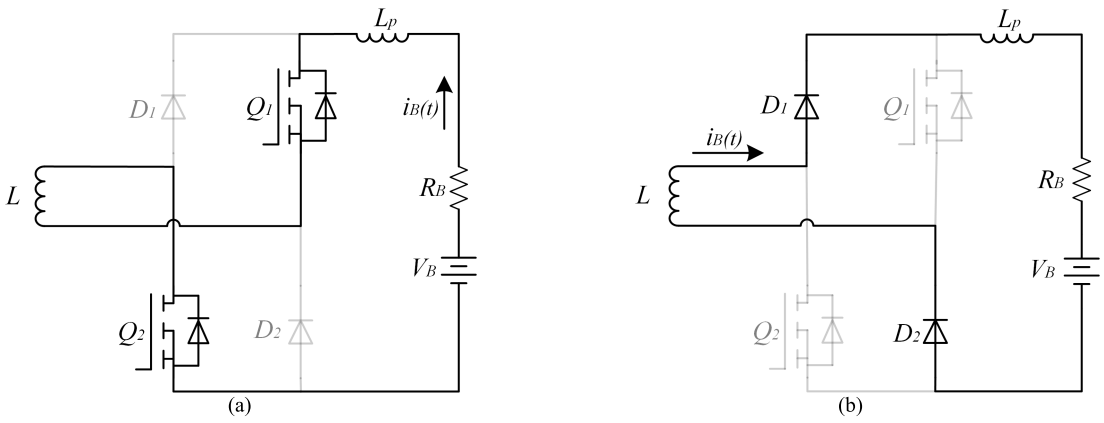

Fig. 3. Operating modes of the H-bridge heating circuit. (a) Mode 1. (b) Mode 2.

switching cycle T_{SW}, i.e.,

$$i_B(t) = \begin{cases} \dfrac{V_B}{R_B}\left(1-\exp\left(-\dfrac{R_B}{L_P+L}t\right)\right), & 0 \le t < \mathrm{DT_{SW}} \\ -\dfrac{V_B}{R_B}\left(2-\exp\left(-\dfrac{R_B}{L_P+L}\mathrm{DT_{SW}}\right)\right) & \\ \exp\left(-\dfrac{R_B}{L_P+L}(t-\mathrm{DT_{SW}})\right)+\dfrac{V_B}{R_B}, & \mathrm{DT_{SW}} \le t < T_{\mathrm{SW}}. \end{cases} \tag{7}$$

Under high-frequency conditions, t tends to be zero, and thus, (7) can be reduced to

$$i_B(t) = \begin{cases} \dfrac{V_B}{L_P+L}t, & 0 \le t < \mathrm{DT_{SW}} \\ -\dfrac{V_B}{L_P+L}\left(1+\dfrac{R_B}{L_P+L}\cdot\mathrm{DT_{SW}}\right) & \\ (t-\mathrm{DT_{SW}})+\dfrac{V_B}{L_P+L}\mathrm{DT_{SW}}, & \mathrm{DT_{SW}} \le t < T_{\mathrm{SW}}. \end{cases} \tag{8}$$

According to (8), the rms current $i_{B,\mathrm{rms}}$ in one switching period T_{SW} can be calculated by (9), as shown at the bottom of the page.

Under the high-frequency conditions, (9) can be simplified to

$$i_{B,\mathrm{rms}} = \frac{V_B D}{\sqrt{3}(L_P+L)f}. \tag{10}$$

It can be seen from (10) that $i_{B,\mathrm{rms}}$ is affected by the switching frequency f, duty cycle D, series inductance L in the circuit, and the voltage V_B of the battery pack. Therefore, without changing the hardware parameters, in Section IV, we will keep V_B/f constant to study the influence of a different switching frequency f on the heating effect under the same rms current. Furthermore, to study the effect of different rms currents on the heating effect at the same frequency, the switching frequency f and duty cycle D will be kept constant, while the battery voltage V_B will be adjusted.

C. Heat Generation Model Under High-Frequency AC

In the literature, a thermal model based on the simplified Bernard heat generation model [32] is usually used to investigate the thermal behavior of the Li-ion battery under ac excitation, i.e.,

$$mc\frac{dT}{dt} = i_{B,\mathrm{rms}}^2 \cdot Z_{\mathrm{Re}} - h \cdot S \cdot (T - T_{\mathrm{amb}}) \tag{11}$$

where m is the battery mass, c is the specific heat capacity, and T represents the battery temperature. The first term on the RHS of (11) represents the Joule heat due to the ohmic resistance, where Z_{Re} is the real part of the battery impedance Z, which can be obtained by electrochemical impedance spectroscopy (EIS). The second term on the RHS of (11) is the heat transferred between the battery and the environment, where h is the heat transfer coefficient, S is the battery surface area, and T_{amb} is the ambient temperature. This lumped thermal equation is valid for the 18 650 cell used in this experiment. This is because, in the experiment, natural convection and low-rate rms current (1.17 and 1.56 C) were applied; under those conditions, the temperature difference between the internal and surface temperatures is normally negligible [33].

$$i_{B,\mathrm{rms}} = \sqrt{\frac{\int_0^{\mathrm{DT_{SW}}}\left[\frac{V_B}{R_B}\left(1-\exp\left(-\frac{R_B}{L_P+L}t\right)\right)\right]^2 dt + \int_{\mathrm{DT_{SW}}}^{T_{\mathrm{SW}}}\left[-\frac{V_B}{L_P+L}\left(1+\frac{R_B}{L_P+L}\cdot\mathrm{DT_{SW}}\right)(t-\mathrm{DT_{SW}})+\frac{V_B}{L_P+L}\mathrm{DT_{SW}}\right]^2 dt}{T_{\mathrm{SW}}}}$$
$$\approx \frac{V_B}{\sqrt{3}R_B}\left(1-\exp\left(-\frac{R_B}{L_P+L}\mathrm{DT_{SW}}\right)\right) \tag{9}$$

In (11), since only Joule heat is considered the source of the heat generation, the heating rate of the battery is proportional to the square of the rms current and the internal resistance. However, we observed that the temperature rise curve calculated by (11) cannot fit the experimental results well, which indicates that, when the battery is excited by high-frequency ac, there should be a portion of the heat that is not generated according to the Joule effect. In this study, an improved thermal model is established to better describe the dynamics of the Li-ion battery under high-frequency ac heating conditions, i.e.,

$$mc\frac{dT}{dt} = i_{B,\mathrm{rms}}^2 \cdot Z_{\mathrm{Re}} - h \cdot S \cdot (T - T_{\mathrm{amb}}) + Q_E \tag{12}$$

where Q_E is an electrochemical heat generation term under ac high-frequency excitation. The experimental results show that Q_E accounts for a certain part of the heat generation of high-frequency batteries, and it is positively correlated with the rms current and the frequency of ac flowing through the battery. We will present the experiment results and the validation process in the later sections.

First, according to (12), the electrochemical heat generation Q_E can be expressed as:

$$Q_E = mc\frac{dT}{dt} + h \cdot S \cdot (T - T_{\mathrm{amb}}) - i_{B,\mathrm{rms}}^2 \cdot Z_{\mathrm{Re}} \tag{13}$$

where the battery temperature T, the rate of change of temperature dT/dt, the rms current $i_{B,\mathrm{rms}}$, and the impedance Z_{Re} can all be readily measured or calculated, and thus, this equation can be used to fit Q_E using well-designed experimental results. Since it is challenging to model this Q_E using first-principle approaches, which requires in-depth knowledge of the mechanisms of various electrochemical reactions, an empirical model will be developed in this work. As will be shown in the later sections, our experimental results exhibit that, under high-frequency excitation, Q_E is correlated with the frequency and the rms value of the current flowing through the battery. We use a binomial to approximate Q_E, i.e.,

$$Q_E = \sum_{m=0}^{2}\sum_{n=0}^{1}\left(a_{mn} \cdot f^m \cdot i_{B,\mathrm{rms}}^n\right) \tag{14}$$

where a_{mn} are six coefficients. The fit coefficients in this work are $a_{00} = -0.1588$, $a_{01} = 3.73 \times 10^{-2}$, $a_{10} = -1.66 \times 10^{-4}$, $a_{11} = 6.235 \times 10^{-5}$, $a_{20} = -1.089 \times 10^{-10}$, and $a_{21} = 0$. It should be pointed out that the fitting relationship given by (14) only comes from limited samples and experiments, and (14) is not universal and cannot be simply applied to other batteries.

Furthermore, according to (10) and (12), the heat generation model under high-frequency ac of the battery can be expressed as

$$mc\frac{dT}{dt} = \frac{V_B^2 D^2}{3(L_P + L)^2 \cdot f^2} \cdot Z_{\mathrm{Re}} - h \cdot S \cdot (T - T_{\mathrm{amb}}) + Q_E. \tag{15}$$

Solving (15) yields the expression of the battery temperature in the time domain, i.e.,

$$T = (T_{\mathrm{amb}} - A) \cdot \exp(-Bt) + A \tag{16}$$

where

$$A = \frac{\frac{V_B^2 D^2}{3(L_P+L)^2 \cdot f^2} \cdot Z_{\mathrm{Re}} + h \cdot S \cdot T_{\mathrm{amb}} + Q_E}{hS} \tag{17}$$

$$B = \frac{hS}{mc}. \tag{18}$$

Equations (16)−(18) will be used next to identify the relationships between the electrochemical generation and various factors in the model.

TABLE I
SPECIFICATION OF LI-ION BATTERY CELL UNDER TEST

Parameter	Symbol	Value
Battery mass	m	47.0 g
Battery surface area	S	4.18×10^{-3} m^2
Operating voltage	V	4.0 V
Rated capacity	-	2900 mAh
Specific heat capacity	c	1.618 J·g·K^{-1}
Series inductance	L	50 μH
Line parasitic inductance	L_P	27 μH

III. EXPERIMENTAL PLATFORM

The heating experimental platform for the 18 650 Li-ion battery was set up, as shown in Fig. 4. The testing platform consists of a climate chamber, a temperature acquisition recorder, an infrared thermal imager (Fluke Ti400), an oscilloscope, a Hall current clamp, and a workstation. The switches Q_1 and Q_2 are implemented by two IMZA65R048M1H MOSFETs. Table I provides the specification of the Li-ion battery cell used in the experiment, where the specific heat capacity c of the battery is determined according to [34]. The real part Z_{Re} of the battery impedance was obtained via EIS.

Under a similar experimental condition, Shang *et al.* [35] show that the temperature distribution of a common 18 650 Li-ion cell is uniform. Hence, it is sufficiently reasonable to use the surface temperature to represent the cell temperature, and thus, a T-type thermocouple was attached to the middle of the battery surface to measure the battery temperature. During the experiment, the battery is first cooled toward a low-temperature set point (e.g., −10 °C) for 3 h before a thermal balance has achieved. The battery is then heated with the ac generated by the designed heating circuit. The heating process terminates either when the measured battery temperature reaches 5 °C or when the heating time is over 15 min.

A. Calibration of Equivalent Heat Transfer Coefficient

The heat dissipation of the battery is described by the equivalent heat transfer coefficient h. Since the value of h is usually determined by various factors, calibration is needed for the experiments. In the heating experiment, the battery was wrapped by a carton to reduce the influence of the fan convection in the climate chamber on the results, and we calibrated h according to the cooling curve when the battery is heated to a high temperature [36]. Since the equivalent heat transfer coefficient h affects the heating rate, the relationship

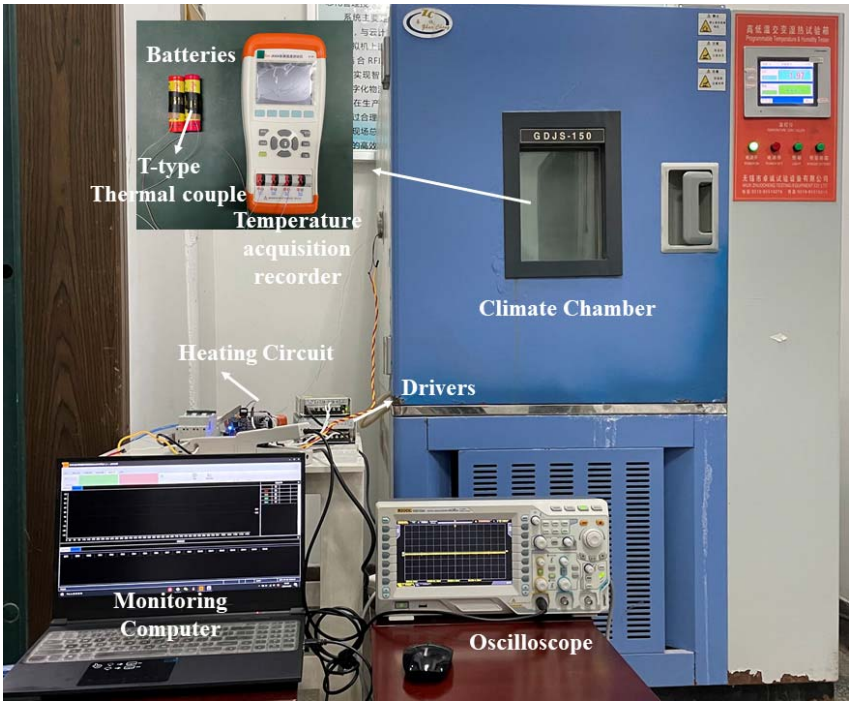

Fig. 4. Experimental setup for 18 650 Li-ion battery preheating.

can be investigated using

$$mc\frac{dT}{dt} = Q - h \cdot S \cdot (T - T_{\text{amb}}). \tag{19}$$

The calibration was carried out according to the cooling curve of the battery cooled from 10 °C to −20 °C. During the cooling process, the heat generation rate of the battery is zero, i.e., $Q = 0$, and thus, (19) can be written as

$$mc\frac{dT}{dt} = -h \cdot S \cdot (T - T_{\text{amb}}). \tag{20}$$

By treating the heating curve as piecewise linear, the equivalent heat transfer coefficient h in a certain temperature range can be considered constant, and thus, (20) can be solved by

$$\ln(T - T_{\text{amb}}) = -\frac{hS}{mc}t + C \tag{21}$$

where C is a constant that can be determined from the initial condition. The equivalent heat transfer coefficient h can then be obtained according to the slope of the curve that describes the relationship between $\ln(T - T_{\text{amb}})$ and the time t.

B. EIS Measurement

In order to obtain the impedance characteristics of the battery, the impedance spectra of the battery were measured at 0 °C, −10 °C, and −20 °C, respectively. In the frequency range of 200 Hz–90 kHz, the ac impedance spectra of 3.1 A at 0 °C, −10 °C, and −20 °C were measured.

The testing equipment is the Bio-logic electrochemical workstation (VMP-300), as shown in Fig. 5. The VMP-300 electrochemical workstation has four channels, up to 16 channels can be expanded, and each channel can be used in parallel. The control voltage is ±10 V, and it can be boosted up to ±48 V. The impedance test ranges are 10 μHz–3 MHz (1%, 1°) and 10 μHz–7 MHz (3%, 3°). The maximum voltage and current resolutions are 1 μV and 760 fA, respectively. The software EC-Lab was used to design the experiments and analyze the measured data.

Fig. 5. Bio-logic VMP-300 electrochemical workstation for EIS measurement.

The EIS testing process of the 18 650 Li-ion battery is described as follows. First, the battery was rested at 0 °C for 6 h, and the ac impedance spectrum of 3.1-A current was tested in the frequency range of 200 Hz–90 kHz. Next, the battery was placed at −10 °C and −20 °C, consecutively, both for 12 h. The ac impedance spectrum of 3.1-A current was measured in the same frequency range as described earlier. Finally, the EIS test was completed by placing the battery at room temperature for 12 h; 27 data points were collected at each temperature.

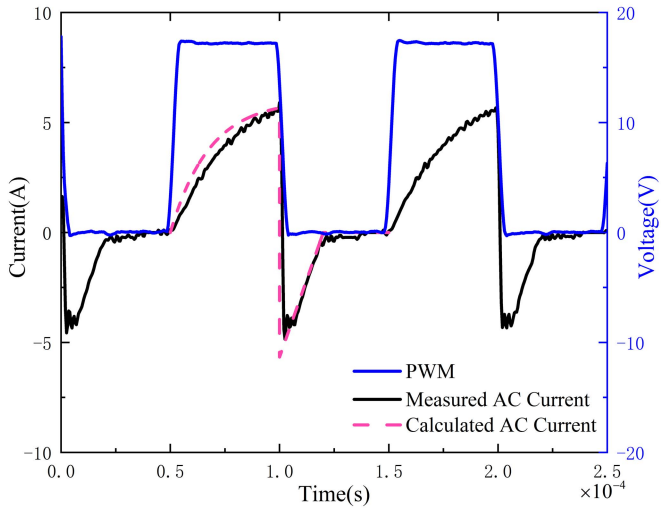

Fig. 6. PWM signal and waveform of the heating current at $f = 10$ kHz and $D = 50\%$.

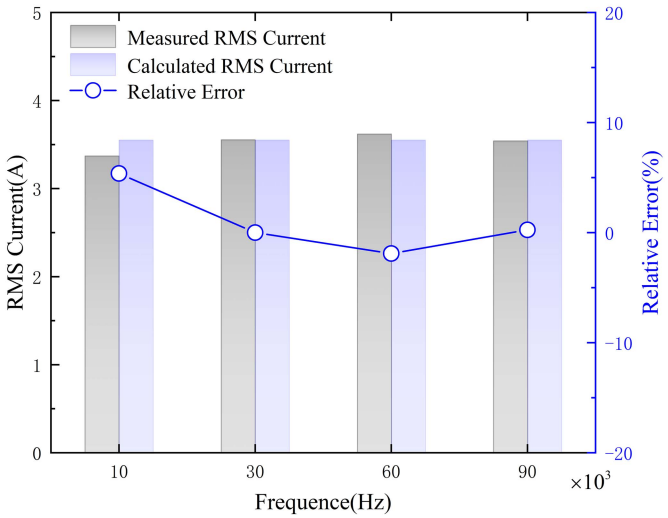

Fig. 7. Comparison of the measured and calculated rms currents at different frequencies.

IV. Results and Discussion

A. Heating Current Waveform and RMS

Fig. 6 shows the waveforms of the measured and calculated heating currents and the PWM signal under the condition of $f = 10$ kHz and $D = 50\%$. It should be noted that, as shown in Fig. 6, when the MOSFET is turned off, the direction of the heating current changes rapidly with the magnitude being reduced slightly, followed by a gradually decreased trend in the magnitude. This is due to the parasitic inductance in the circuit, which can hinder the change in the current. Furthermore, it can be seen that, in each switching period, there is a short-time damped oscillation in the reversed current, and this phenomenon is caused by the *LC* resonant circuit formed by the drain–source capacitance of MOSFETs and the line inductance. It can also be seen from Fig. 6 that the calculated heating current from (7) is in good agreement with the measured one.

Fig. 7 shows the rms currents measured and calculated at different switching frequencies. It can be seen that the rms currents measured at the four frequencies are almost the same, all about 3.51 A. Hence, this result shows that one can maintain a certain V_B/f ratio to generate an expected rms current under varying frequency conditions. In addition, it can be seen that, at all switching frequencies, the relative errors between the theoretical and the actual rms values are within 6%. The largest relative error is 5.37% when the switching frequency is 10 kHz, and this is due to the fact that the assumption that the frequency period is close to zero is less valid in this condition. The small errors are acceptable, which validates the rms current expression (10).

TABLE II
Calibration Result of the Convective Heat Transfer Coefficient

Temperature Range (°C)	h (W·m^{-2}·K^{-1})
0 to 10	11.29
−10 to 0	12.7
−15 to −10	10.01
−20 to −15	11.34

B. Calibration Results of Convective Heat Transfer Coefficient

Fig. 8(a) depicts the waveform of temperature versus time when the battery is being cooled from 10 °C to −20 °C. Based on this curve, we obtain the $\ln(T - T_{amb})$ versus time relationship, and the results are plotted in Fig. 8(b). It can be seen from Fig. 8 that, during the whole cooling process, the rates of change of both curves are not constant, indicating that h has changed at different battery temperatures. At a high battery temperature, the corresponding h is large, and thus, the effect of the heat transfer between the battery and the external environment is more significant. Hence, this curve is fit by a piecewise linear function with different coefficients h in each segment, as provided in Table II.

C. EIS Test Results

The relationships between the impedance and the frequency at different temperatures are plotted in Fig. 9, measured from the EIS test. Fig. 9(a) depicts the relationship between the real part Z_{Re} of the impedance and the frequency, and Fig. 9(b) depicts the relationship between the magnitude $|Z|$ of the impedance and the frequency.

From the EIS results, we have the following findings.

1) With the increase in temperature, the impedance of the battery decreases significantly.

2) At the same temperature, there is a decreasing trend in the magnitude of the impedance at the low-frequency region as the frequency increases, but the magnitude of the impedance increases at the high-frequency region.

3) At the same temperature, the real part of the cell impedance does not change significantly in the high-frequency region. In other words, in this experiment, the change of the real part of battery impedance Z_{Re} can be ignored in the high-frequency region.

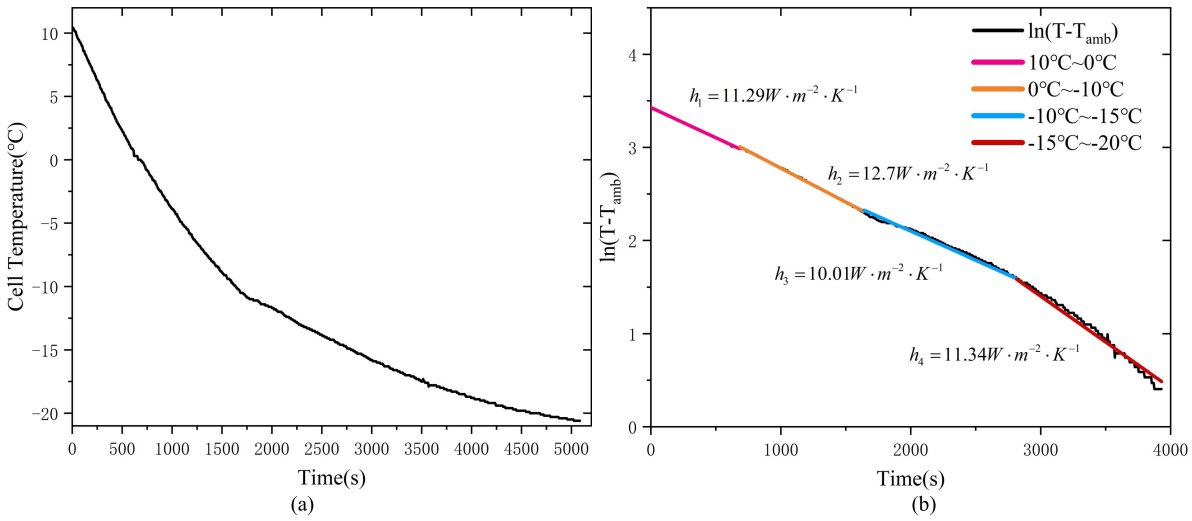

Fig. 8. Calibration results of the convective heat transfer coefficient. (a) Battery temperature curve under a cooling condition. (b) Curve of $\ln(T - T_{\text{amb}})$.

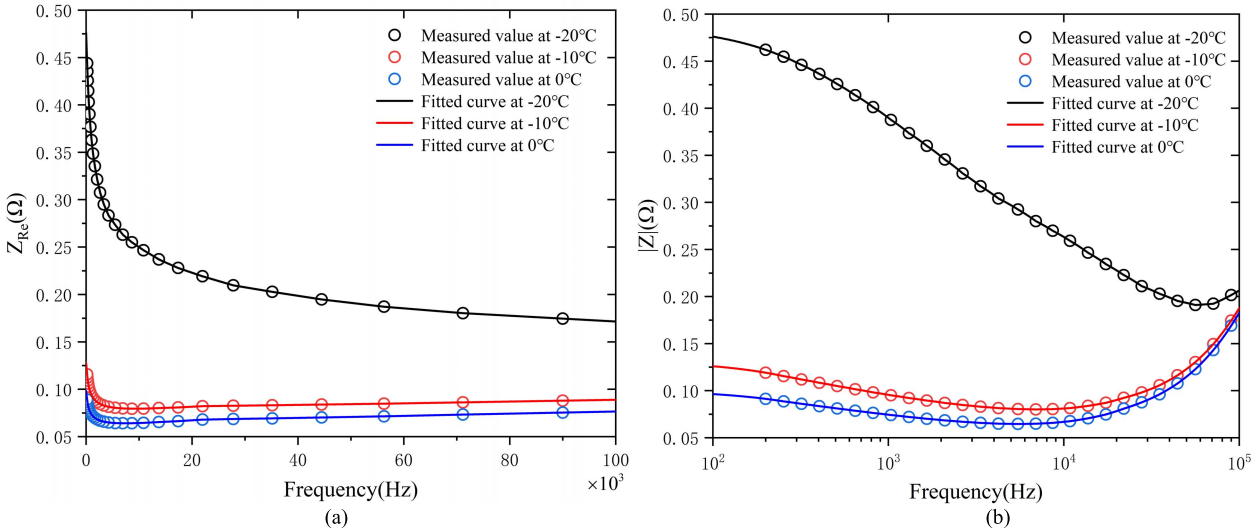

Fig. 9. EIS test results. (a) Relationship between the real part Z_{Re} of the battery impedance and the frequency at different temperatures. (b) Relationship between the magnitude $|Z|$ of the impedance and the frequency at different temperatures.

D. Comparison of Temperature Rise Under Different Switching Frequencies

In this work, four different switching frequencies were used for ac heating, while rms currents were maintained as 1.17 C (3.51 A), aiming to study the influence of switching frequencies. The heating time and rates, the average values of electrochemical heat generation Q_E, and the energy consumption at different switching frequencies and different ambient temperatures are provided in Table III. Fig. 10 presents the heating results of different switching frequencies when the ambient temperature is -10 °C, where it can be seen that the heating rate of the battery can be significantly improved by increasing the switching frequency. Specifically, at $f = 10$ kHz, it takes 10.17 min for the heating circuit to raise the battery's temperature to 5 °C with about 5.45% energy loss, and the average temperature rise rate is 1.47 °C/min. When the switching frequency is increased to $f = 90$ kHz, the heating time is shortened to 3.58 min, and a high average temperature rise rate of 4.19 °C/min is achieved, and in this case, about 2.69% of the cell energy is consumed.

Fig. 10(a) compares the calculated heating curves of the battery using the thermal model based on the simplified Bernard heat generation model, and it can be seen that there are significant errors between the model and the measurements. Particularly, with the increase in the switching frequency, the error of the predictive results of the model increases, and this does not comply with the observation of the actual temperature rise. On the contrary, by using the proposed equation (16), the heating curves in Fig. 10(b) show that the calculated results are in good agreement with the experiments, which validates the electrochemical heat generation term during the high-frequency heating process.

A similar comparison was done when the ambient temperature was set to -20 °C, and the results are shown in Fig. 11. From the experiment results, it can be seen that, when the switching frequency is 10 kHz, the battery temperature can

TABLE III
HEATING EFFECT AT DIFFERENT SWITCHING FREQUENCIES

Ambient Temperature (°C)	Switching Frequency (kHz)	Heating Time (min)	Average Heating Rate (°C/min)	Average Electrochemical Heat Generation Q_E (W)	Energy Consumption (%)
-10	10	10.17	1.47	0.382	5.45
	30	5.75	2.61	1.698	3.93
	60	4.75	3.16	2.559	3.41
	90	3.58	4.19	3.905	2.69
-20	10	15	1.33	0.394	9.93
	30	9.33	2.68	2.115	6.41
	60	8.25	3.03	2.517	5.59
	90	7.33	3.41	2.962	5.34

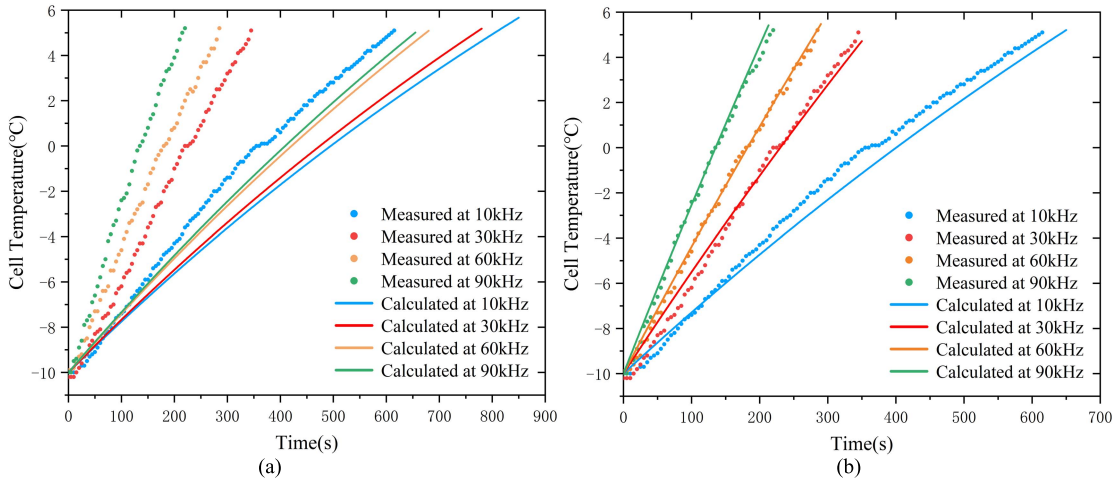

Fig. 10. Heating results of different switching frequencies when the ambient temperature is −10 °C. (a) Prediction results of the simplified Bernard heat generation model. (b) Model prediction results considering Q_E.

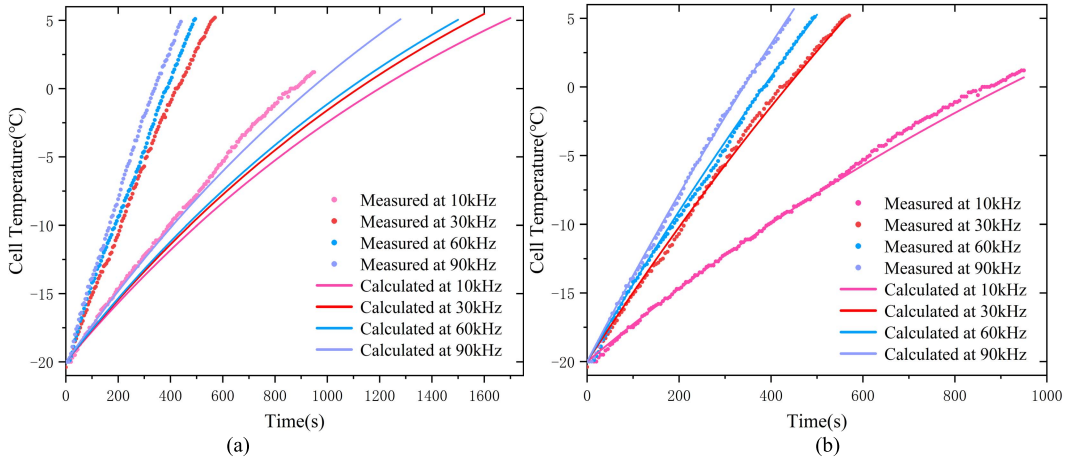

Fig. 11. Heating results of different switching frequencies when the ambient temperature is −20 °C. (a) Prediction results of the simplified Bernard heat generation model. (b) Model prediction results considering Q_E.

only be increased to 0.1 °C after 15 min. The corresponding average heating rate is 1.33 °C/min, and about 9.93% of the cell energy is consumed during heating. Once the switching frequency was increased to 30 kHz, the battery temperature can rise to 5 °C in 9.33 min, and the average heating rate is doubled to 2.68 °C/min. By comparing Fig. 11(a) and (b),

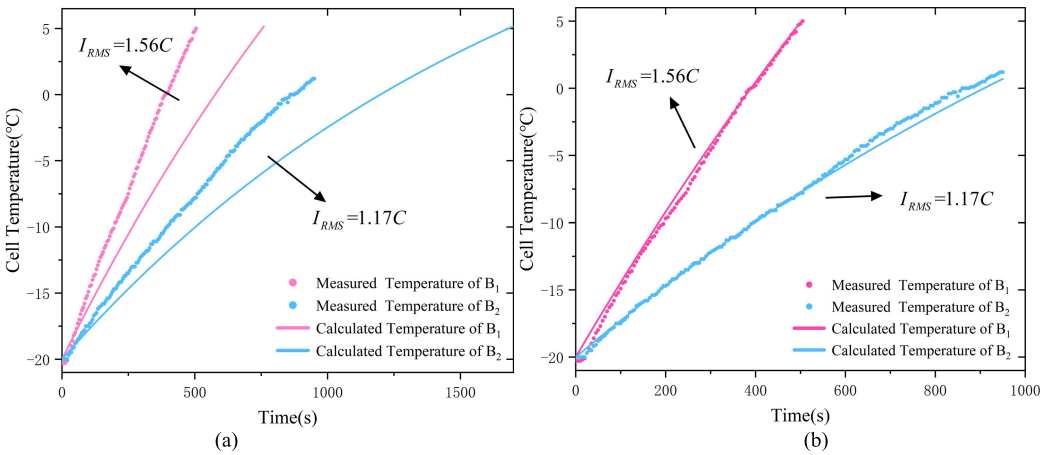

Fig. 12. Heating results of different rms currents at −20 °C and 10 kHz. (a) Prediction results of the simplified Bernard heat generation model. (b) Model prediction results considering Q_E.

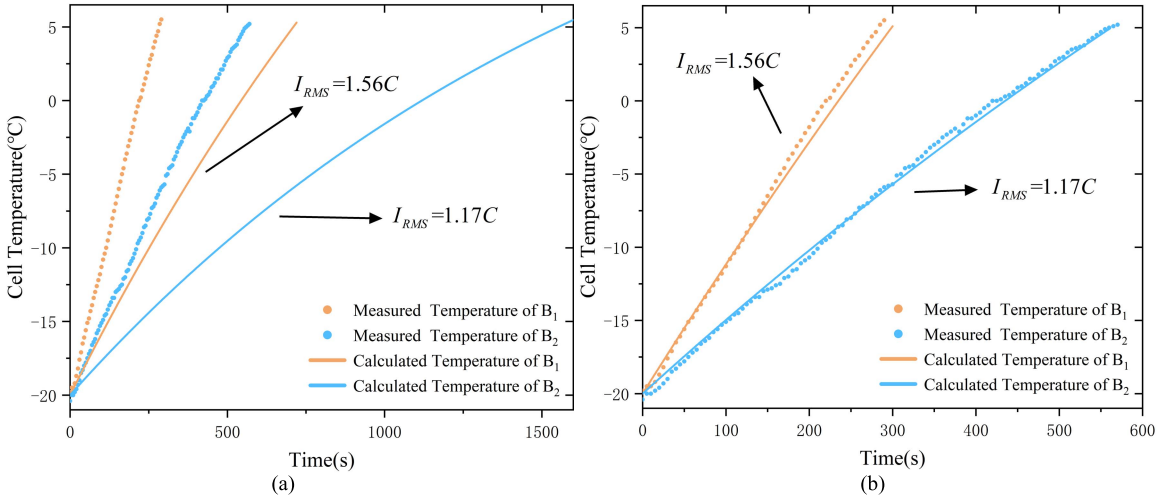

Fig. 13. Heating results of different rms currents at −20 °C and 30 kHz. (a) Prediction results of the simplified Bernard heat generation model. (b) Model prediction results considering Q_E.

TABLE IV
HEATING EFFECT OF BATTERIES UNDER DIFFERENT RMS CURRENTS

Ambient Temperature (°C)	Switching Frequency (kHz)	RMS Current (C-Rate)	Heating Time (min)	Average Heating Rate (°C/min)	Average Electrochemical Heat Generation Q_E (W)	Energy Consumption (%)
−20	10	1.17	15	1.33	0.394	9.93
		1.56	8.41	2.97	1.256	7.07
	30	1.17	9.33	2.68	2.115	6.41
		1.56	4.67	5.36	3.672	5.48

it can be seen that the prediction results based on the proposed heat generation are accurate and much improved from that using the conventional model.

In addition, from Table III, it can be seen that, at the same temperature, the average electrochemical heat generation is positively correlated with the switching frequency. The experimental results show that electrochemical heat generation exists in the high-frequency ac heating process of the battery. For the same rms current, the average electrochemical heat generation can be increased by increasing the switching frequency so that the heating performance of the battery can be significantly improved.

E. Comparison of Temperature Rise Under Different RMS Currents

In order to investigate the effect of the rms value of the heating current on the battery heating performance, two groups of comparative experiments were carried out, based on the frequency of 10 and 30 kHz, respectively. For each

comparison, two rms currents, i.e., 1.17 (3.51) and 1.56 C (4.68 A), were tested, the ambient temperature is −20 °C, and the PWM duty cycle is 50%. The results are plotted in Figs. 12 and 13, and Table IV provides the heating time, heating rate, average values of electrochemical heat generation, and energy consumption.

The experimental results show that the heating rate of the battery can be significantly increased by increasing the rms current at the same switching frequency. When the switching frequency is 10 kHz, the rms current is 1.56 C, and the cell temperature rises to 5 °C in 8.41 min. In this process, about 7.07% of the cell energy is consumed. Compared with 1.17 C, the average heating rate is 2.23 times higher. When the switching frequency is 30 kHz, the rms current is 1.56 C, and the battery's temperature rises to 5 °C in 4.67 min with about 5.48% cell energy loss. Compared with 1.17 C, the average temperature rise rate is about twice higher, and the heating time is reduced by 50%.

As illustrated in Figs. 12(b) and 13(b), the prediction errors of the heating curves are small when the electrochemical heat generation Q_E is considered. It can be seen from Table IV that, with the same frequency, the average electrochemical heat generation increases with the rms current, and the heating rate of the battery can be increased by increasing the rms current. On the other hand, it should be pointed out that, although a higher rms current can effectively increase the heating rate, excessive rms current can cause aging phenomena, such as Li-ion deposition, and reduce the available capacity of the battery. Therefore, it is necessary to choose an appropriate high-frequency ac to balance the heating rate and the battery health.

V. Conclusion

In this article, a circuit topology based on H-bridge is used to design a self-heating strategy and study thermal characteristics of Li-ion batteries at low temperatures and under high-frequency excitation. The main concluding remarks are given as follows.

1) The heating circuit based on the H-bridge designed in this work can quickly heat the battery by using the battery itself as a power source to generate alternating current without any external source. When the ac frequency is 90 kHz, the battery can be heated from −20 °C to 5 °C in 7.33 min, and the battery energy consumption is only 5.34%.

2) In addition to the ohmic heat generation of the battery, under high-frequency ac excitation, the heat source also contains an electrochemical heat generation part. By increasing the electrochemical heat generation from 0.382 to 3.905 W, the average heating rate can be increased by a factor of 2.85. Therefore, increasing the electrochemical heat generation can effectively increase the heating rate.

3) Increasing the ac frequency and rms of the current can significantly increase the electrochemical heat generation and, thus, the heating rate of the battery.

The present experiment has some limitations due to the presence of parasitic inductance in the H-bridge heat circuit, which can cause energy losses. Further improvements can be made by reducing the parasitic inductance of the wire and the switching loss of the MOSFET with a better circuit design. Furthermore, since the heat generation of Li-ion batteries is a complex electrochemical reaction process, a suitable physics-based model for electrochemical heat generation shall be established by investigating the mechanisms in our future work to accurately predict the heating characteristics of the battery under high-frequency excitation.

References

[1] J. Tian, R. Xiong, W. Shen, J. Lu, and X.-G. Yang, "Deep neural network battery charging curve prediction using 30 points collected in 10 min," *Joule*, vol. 5, no. 6, pp. 1521–1534, Jun. 2021, doi: 10.1016/j.joule.2021.05.012.

[2] Z. Wei, J. Zhao, R. Xiong, G. Dong, J. Pou, and K. J. Tseng, "Online estimation of power capacity with noise effect attenuation for lithium-ion battery," *IEEE Trans. Ind. Electron.*, vol. 66, no. 7, pp. 5724–5735, Jul. 2019.

[3] C. Zhu, Y. Cao, H. Zhang, F. Lu, and X. Zhang, "Comprehensive design and optimization of an onboard resonant self-heater for EV battery," *IEEE Trans. Transport. Electrific.*, vol. 7, no. 2, pp. 452–463, Jun. 2021.

[4] K. Liu, C. Zou, K. Li, and T. Wik, "Charging pattern optimization for lithium-ion batteries with an electrothermal-aging model," *IEEE Trans. Ind. Informat.*, vol. 14, no. 12, pp. 5463–5474, Dec. 2018.

[5] R. Xiong, J. Wang, W. Shen, J. Tian, and H. Mu, "Co-estimation of state of charge and capacity for lithium-ion batteries with multi-stage model fusion method," *Engineering*, Feb. 2021, doi: 10.1016/j.eng.2020.10.022.

[6] X. W. Zhao, G. Y. Zhang, L. Yang, J. X. Qiang, and Z. Q. Chen, "A new charging mode of Li-ion batteries with LiFePO4/C composites under low temperature," *J. Thermal Anal. Calorimetry*, vol. 104, no. 2, pp. 561–567, May 2011.

[7] Y. Li *et al.*, "Electrochemical model-based fast charging: Physical constraint-triggered PI control," *IEEE Trans. Energy Convers.*, early access, Mar. 17, 2021, doi: 10.1109/TEC.2021.3065983.

[8] X. Hu, Y. Zheng, D. A. Howey, H. Perez, A. Foley, and M. Pecht, "Battery warm-up methodologies at subzero temperatures for automotive applications: Recent advances and perspectives," *Prog. Energy Combustion Sci.*, vol. 77, Mar. 2020, Art. no. 100806.

[9] J. Jaguemont, L. Boulon, and Y. Dubé, "A comprehensive review of lithium-ion batteries used in hybrid and electric vehicles at cold temperatures," *Appl. Energy*, vol. 164, pp. 99–114, Feb. 2016.

[10] M.-T.-F. Rodrigues *et al.*, "A materials perspective on Li-ion batteries at extreme temperatures," *Nature Energy*, vol. 2, no. 8, pp. 359–367, Aug. 2017.

[11] R. Yang, R. Xiong, W. Shen, and X. Lin, "Extreme learning machine-based thermal model for lithium-ion batteries of electric vehicles under external short circuit," *Engineering*, vol. 7, no. 3, pp. 395–405, Mar. 2021.

[12] K. Liu, X. Hu, Z. Wei, Y. Li, and Y. Jiang, "Modified Gaussian process regression models for cyclic capacity prediction of lithium-ion batteries," *IEEE Trans. Transport. Electrific.*, vol. 5, no. 4, pp. 1225–1235, Dec. 2019.

[13] G. Zhu *et al.*, "Materials insights into low-temperature performances of lithium-ion batteries," *J. Power Sources*, vol. 300, pp. 29–40, Dec. 2015.

[14] C. Zhang, J. Jiang, Y. Gao, W. Zhang, Q. Liu, and X. Hu, "Charging optimization in lithium-ion batteries based on temperature rise and charge time," *Appl. Energy*, vol. 194, pp. 569–577, May 2017.

[15] Z. Lei, C. Zhang, J. Li, G. Fan, and Z. Lin, "Preheating method of lithium-ion batteries in an electric vehicle," *J. Modern Power Syst. Clean Energy*, vol. 3, no. 2, pp. 289–296, Jun. 2015.

[16] S. Mohan, J. Siegel, A. G. Stefanopoulou, M. Castanier, and Y. Ding, "Synthesis of an energy-optimal self-heating strategy for Li-ion batteries," in *Proc. IEEE 55th Conf. Decis. Control (CDC)*, Dec. 2016, pp. 1589–1594.

[17] Y. Ji and C. Y. Wang, "Heating strategies for Li-ion batteries operated from subzero temperatures," *Electrochim. Acta*, vol. 107, pp. 664–674, Sep. 2013.

[18] S. Wu, R. Xiong, H. Li, V. Nian, and S. Ma, "The state of the art on preheating lithium-ion batteries in cold weather," *J. Energy Storage*, vol. 27, Feb. 2020, Art. no. 101059.

[19] C.-Y. Wang *et al.*, "Lithium-ion battery structure that self-heats at low temperatures," *Nature*, vol. 529, pp. 515–518, Jan. 2016.

[20] W. Tao, K. J. Tseng, J. Zhao, and Z. Wei, "Thermal investigation of lithium-ion battery module with different cell arrangement structures and forced air-cooling strategies," *Appl. Energy*, vol. 134, pp. 229–238, Dec. 2014.
[21] X.-G. Yang, G. Zhang, and C.-Y. Wang, "Computational design and refinement of self-heating lithium ion batteries," *J. Power Sources*, vol. 328, pp. 203–211, Oct. 2016.
[22] G. Zhang, S. Ge, T. Xu, X.-G. Yang, H. Tian, and C.-Y. Wang, "Rapid self-heating and internal temperature sensing of lithium-ion batteries at low temperatures," *Electrochim. Acta*, vol. 218, pp. 149–155, Nov. 2016.
[23] Y. Qin *et al.*, "A rapid lithium-ion battery heating method based on bidirectional pulsed current: Heating effect and impact on battery life," *Appl. Energy*, vol. 280, Dec. 2020, Art. no. 115957.
[24] S. Mohan, Y. Kim, and A. G. Stefanopoulou, "Energy-conscious warm-up of Li-ion cells from subzero temperatures," *IEEE Trans. Ind. Electron.*, vol. 63, no. 5, pp. 2954–2964, May 2016.
[25] J. Zhang, H. Ge, Z. Li, and Z. Ding, "Internal heating of lithium-ion batteries using alternating current based on the heat generation model in frequency domain," *J. Power Sources*, vol. 273, pp. 1030–1037, Jan. 2015.
[26] H. Ruan *et al.*, "A rapid low-temperature internal heating strategy with optimal frequency based on constant polarization voltage for lithium-ion batteries," *Appl. Energy*, vol. 177, pp. 771–782, Sep. 2016.
[27] H. Ge, J. Huang, J. Zhang, and Z. Li, "Temperature-adaptive alternating current preheating of lithium-ion batteries with lithium deposition prevention," *J. Electrochem. Soc.*, vol. 163, no. 2, pp. A290–A299, 2016.
[28] J. Jiang, H. Ruan, B. Sun, L. Wang, W. Gao, and W. Zhang, "A low-temperature internal heating strategy without lifetime reduction for large-size automotive lithium-ion battery pack," *Appl. Energy*, vol. 230, pp. 257–266, Nov. 2018.
[29] Y. Shang, K. Liu, N. Cui, Q. Zhang, and C. Zhang, "A sine-wave heating circuit for automotive battery self-heating at subzero temperatures," *IEEE Trans. Ind. Informat.*, vol. 16, no. 5, pp. 3355–3365, May 2020.
[30] J. Jiang *et al.*, "A reduced low-temperature electro-thermal coupled model for lithium-ion batteries," *Appl. Energy*, vol. 177, pp. 804–816, Sep. 2016.
[31] Y. Shang, C. Zhu, G. Lu, Q. Zhang, N. Cui, and C. Zhang, "Modeling and analysis of high-frequency alternating-current heating for lithium-ion batteries under low-temperature operations," *J. Power Sources*, vol. 450, Feb. 2020, Art. no. 227435.
[32] B. Wu, Z. Li, and J. Zhang, "Thermal design for the pouch-type large-format lithium-ion batteries: I. Thermo-electrical modeling and origins of temperature non-uniformity," *J. Electrochem. Soc.*, vol. 162, no. 1, pp. A181–A191, 2015.
[33] G. Zhang, L. Cao, S. Ge, C.-Y. Wang, C. E. Shaffer, and C. D. Rahn, "*In situ* measurement of radial temperature distributions in cylindrical Li-ion cells," *J. Electrochem. Soc.*, vol. 161, no. 10, pp. A1499–A1507, 2014.
[34] S. J. Drake, D. A. Wetz, J. K. Ostanek, S. P. Miller, J. M. Heinzel, and A. Jain, "Measurement of anisotropic thermophysical properties of cylindrical Li-ion cells," *J. Power Sources*, vol. 252, pp. 298–304, Apr. 2014.
[35] Y. Shang, B. Xia, N. Cui, C. Zhang, and C. C. Mi, "An automotive onboard AC heater without external power supplies for lithium-ion batteries at low temperatures," *IEEE Trans. Power Electron.*, vol. 33, no. 9, pp. 7759–7769, Sep. 2018.
[36] X. Wu, Z. Cui, E. Chen, and J. Du, "Capacity degradation minimization oriented optimization for the pulse preheating of lithium-ion batteries under low temperature," *J. Energy Storage*, vol. 31, Oct. 2020, Art. no. 101746.

Zhongxiaobang Hu received the B.E. degree in electrical engineering and its automation from Hubei University of Technology, Wuhan, China, in 2019. He is currently pursuing the M.S. degree with the School of Automation, Wuhan University of Technology, Wuhan.

His research interests include lithium-ion power battery warm-up strategy and battery management systems.

Yang Li (Member, IEEE) received the B.E. degree in electrical engineering from Wuhan University, Wuhan, China, in 2007, and the M.Sc. and Ph.D. degrees in power engineering from Nanyang Technological University (NTU), Singapore, in 2008 and 2015, respectively.

From 2015 to 2016, he was a Research Fellow with the Energy Research Institute, NTU. From 2016 to 2018, he was a Research Fellow with the School of Electrical Engineering and Computer Science, Queensland University of Technology, Brisbane, QLD, Australia. Since 2019, he has been an Associate Professor with the School of Automation, Wuhan University of Technology, Wuhan. Since 2020, he has been a Visiting Professor and a Researcher with the Department of Electrical Engineering, Chalmers University of Technology, Gothenburg, Sweden. His research interests include modeling, control, and applications of renewable and energy storage systems in power systems and transport sectors.

Dr. Li was a recipient of the EU Marie Skłodowska-Curie Individual Fellowship in 2020.

Furong Liu (Member, IEEE) received the B.S. and M.S. degrees in automation from Wuhan University of Science and Technology, Wuhan, China, in 1989 and 1998, respectively, and the Ph.D. degree in electrical engineering from the Huazhong University of Science and Technology, Wuhan, in 2008.

From October 2002 to November 2003, she was a Visiting Scholar with the Department of Energy Technology, Aalborg University, Aalborg, Denmark. She is currently an Associate Professor with the School of Automation, Wuhan University of Technology, Wuhan. She has authored or coauthored about 30 journal articles and conference papers. Her current research interests include thermal management of lithium-ion power batteries, power electronics for renewable energy systems, and electric cars.

Bo Zhao (Member, IEEE) is currently the Dean of the Director of the Energy Internet Technology Laboratory, State Grid Zhejiang Electric Power Research Institute, Hangzhou, China. He is also a professorate senior engineer and an expert in the field of distributed power supply, energy storage, and microgrids.

Weibo Li (Member, IEEE) received the Ph.D. degree in electrical engineering from the Huazhong University of Science and Technology, Wuhan, China, in 2005.

In 2008, engaged in the research and development of a scientific research prototype of a major project at the Post-Doctoral Station of the School of Electrical Engineering, Naval University of Engineering, Wuhan. In 2005, he joined the army as a Core Research Member of the Key Laboratory of Naval Integrated Power Science and Technology, Naval University of Engineering, engaged in undergraduate teaching, scientific research, and post-graduate training. In December 2015, he was transferred to the School of Automation, Wuhan University of Technology, Wuhan, and engaged in undergraduate teaching, scientific research, and post-graduate training.

Ruixin Yang (Member, IEEE) received the Ph.D. degree in mechanical engineering from Beijing Institute of Technology, Beijing, China, in 2020, and the Ph.D. degree in electrical engineering from the Swinburne University of Technology, Melbourne, VIC, Australia, in 2020.

He was a Visiting Scholar with the University of California at Davis, Davis, CA, USA, from November 2018 to February 2019. He currently holds a post-doctoral position at Beijing Institute of Technology. He has published more than ten journal articles and more than six patents since 2015. His research mainly focuses on the thermal and safety management of lithium-ion batteries for electric vehicles.

Dr. Yang was a recipient of the Best Paper Award from the International Conference on Electric and Intelligent Vehicles (ICEIV2018), in Melbourne. He also serves as the Standing Director of the Battery System Subcommittee at the IEEE PES Electric Vehicle Satellite Committee-China.

Changjun Xie (Member, IEEE) received the Ph.D. degree in vehicle engineering from Wuhan University of Technology (WHUT), Wuhan, Hubei, China, in 2009.

From 2012 to 2013, he was a Visiting Scholar with the University of California at Davis (UC Davis), Davis, CA, USA. He is currently a Professor and the Vice-Dean of the School of Automation, WHUT. He has published over 60 articles, and over 50 articles are indexed by SCI or EI. His research interests include battery management systems, control strategy of fuel cell vehicles, and thermoelectric power generation.

Dr. Xie also serves as the Standing Director of the Battery System Subcommittee at the IEEE PES Electric Vehicle Satellite Committee-China.

Ying Shi received the Ph.D. degree in marine engineering from Wuhan University of Technology, Wuhan, Hubei, China, in 2006.

She is currently a Professor of artificial intelligence with Wuhan University of Technology. Her current research interests include big data systems, grid security, machine learning, and deep learning.